

Identification of *N*-(4-Piperidinyl)-4-(2,6-dichlorobenzoylamino)-1*H*-pyrazole-3-carboxamide (AT7519), a Novel Cyclin Dependent Kinase Inhibitor Using Fragment-Based X-Ray Crystallography and Structure Based Drug Design[†]

Paul G. Wyatt,^{‡,∇} Andrew J. Woodhead,^{‡,*} Valerio Berdini,[‡] John A. Boulstridge,[‡] Maria G. Carr,[‡] David M. Cross,[#] Deborah J. Davis,^{||} Lindsay A. Devine,[§] Theresa R. Early,[‡] Ruth E. Feltell,^{||} E. Jonathan Lewis,[#] Rachel L. McMenemy,^{||} Eva F. Navarro,[‡] Michael A. O'Brien,[‡] Marc O'Reilly,[§] Matthias Reule,[#] Gordon Saxty,[‡] Lisa C. A. Seavers,^{||} Donna-Michelle Smith,[#] Matt S. Squires,^{||} Gary Trewartha,[‡] Margaret T. Walker,[‡] and Alison J.-A. Woolford[‡]

Astex Therapeutics Ltd, 436 Cambridge Science Park, Milton Road, Cambridge, CB4 0QA, United Kingdom

Received April 3, 2008

The application of fragment-based screening techniques to cyclin dependent kinase 2 (CDK2) identified multiple (>30) efficient, synthetically tractable small molecule hits for further optimization. Structure-based design approaches led to the identification of multiple lead series, which retained the key interactions of the initial binding fragments and additionally explored other areas of the ATP binding site. The majority of this paper details the structure-guided optimization of indazole (**6**) using information gained from multiple ligand–CDK2 cocrystal structures. Identification of key binding features for this class of compounds resulted in a series of molecules with low nM affinity for CDK2. Optimisation of cellular activity and characterization of pharmacokinetic properties led to the identification of **33** (AT7519), which is currently being evaluated in clinical trials for the treatment of human cancers.

Introduction

Background to Fragment-Based Drug Discovery. Astex has previously described the use of fragment-based X-ray crystallographic screening to identify low-affinity fragment hits for a range of targets,^{1,2} and the area in general has been reviewed extensively over recent years.^{3–7} Fragment-based screening approaches have become widely used throughout the pharmaceutical industry and can now be regarded as a complimentary approach to high-throughput screening. Fragments are low-molecular-weight compounds³ (typically 100–250 Da) with generally low binding affinities (>100 μ M) and, as a result, very sensitive biophysical screening methods are frequently used to detect them, such as X-ray crystallography,^{1,8} nuclear magnetic resonance spectroscopy (NMR),⁹ and surface plasmon resonance (SPR).¹⁰ Fragment screening has a number of advantages over conventional screening methodologies. First, only small libraries of compounds are needed for screening purposes (~200–2000), due to the much greater probability of complementarity between each fragment and the target than is expected for larger, drug-like compounds.¹¹ Second, despite their often very low affinity, fragments generally possess good ligand

efficiency (LE^a)¹² and as such form a small number of very high quality interactions. It is possible to optimize fragments to relatively low molecular weight leads with good drug-like properties, and this can be achieved with a limited number of molecules, particularly if good structural data is available. LE is the ratio of free binding affinity to molecular size, depicted mathematically as $LE = -\Delta G / HAC \approx -RT \ln(IC_{50}) / HAC$, where the HAC (heavy atom count) includes all non-hydrogen atoms. This concept can be used to compare hits of widely differing structures and activities and is also a simple way of determining if the optimization of a hit into a lead has been carried out efficiently.

Inhibition of Cyclin Dependent Kinases. The cyclin-dependent kinases (CDKs) are a family of serine-threonine protein kinases, which are key regulatory elements in cell cycle progression. The activity of CDKs is critically dependent on the presence of their regulatory partners (cyclins), whose levels of expression are tightly controlled throughout the different phases of the cell cycle.^{13–15} Loss of cell cycle control resulting in aberrant cellular proliferation is one of the key characteristics of cancer,¹⁶ and it is anticipated that inhibition of CDKs may provide an effective method for controlling tumor growth and hence an effective weapon in cancer chemotherapy.^{17,18}

CDK2/cyclin E, CDK4/cyclin D and CDK6/cyclin D primarily regulate progression from the G1 (Gap1) phase to the S phase (DNA synthesis) of the cell cycle through phosphorylation of the retinoblastoma protein (Rb).^{19,20} Subsequent progression through S phase and entry into G2 (Gap2) is thought to require the CDK2/cyclin A complex. Complexes of CDK1 and the A or B type cyclins regulate both the G2 to M phase transition

[†] Coordinates of the CDK2 complexes with compounds **6**, **7**, **8**, **10**, **11**, **12**, **14**, **15**, **18**, **22**, **23**, **28**, **29**, and **33** have been deposited in the Protein Data Bank under accession codes 2VTA, 2VTH, 2VTM, 2VTJ, 2VTR, 2VTS, 2VTI, 2VTL, 2VTN, 2VTO, 2VTP, 2VTQ, 2VTT, and 2VU3, together with the corresponding structure factor files.

* To whom correspondence should be addressed. Phone: +44 (0)1223 226287. Fax: +44 (0)1223 226201. E-mail: a.woodhead@astex-therapeutics.com.

[‡] Medicinal Chemistry.

[§] Structural Biology.

^{||} Biology.

[‡] Computational Chemistry and Informatics.

[#] DMPK.

[∇] Current address: Drug Discovery Unit, Division of Biological Chemistry & Drug Discovery College of Life Sciences, James Black Centre, University of Dundee, Dow Street, Dundee, DD1 5EH, United Kingdom. Phone: +44 (0)1382 386231. E-mail: p.g.wyatt@dundee.ac.uk.

^a Abbreviations: CDK, cyclin dependent kinase; DCM, dichloromethane; DFG, region of conserved amino acids, aspartic acid, phenyl alanine, glycine; EDC, 1-(3-dimethylaminopropyl)-3-ethylcarbodiimide; HP β CD, hydroxypropyl- β -cyclodextrin; HOBT, 1-hydroxybenzotriazole hydrate; HOAt, 1-hydroxy-7-azabenzotriazole; LE, ligand efficiency; NMP, 1-methyl-2-pyrrolidinone; NPM, nucleophosmin; Rb, retinoblastoma protein; *T/C*, mean tumor volume of treated animals divided by the mean control tumor volume.

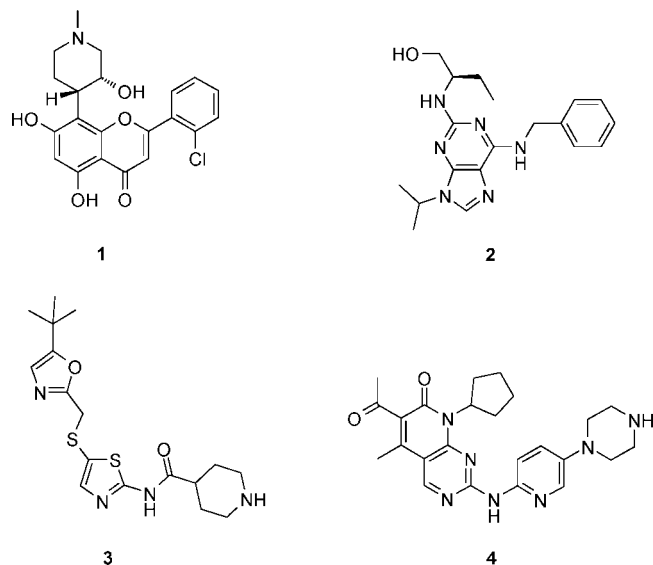


Figure 1. CDK inhibitors currently under investigation in clinical trials.

and mitosis.^{15,17} However, not all members of the CDK family are involved exclusively in cell cycle control; CDK2/cyclin E plays a role in the p53 mediated DNA damage response pathway and also in gene regulation.^{21–24} CDKs 7, 8, and 9 are implicated in the regulation of transcription, and CDK5 plays a role in neuronal and secretory cell function.^{25–27}

Thus inhibiting CDK enzyme activity may affect cell growth and survival via several different mechanisms and therefore represents an attractive target for therapeutics designed to arrest, or recover control of, the cell cycle in aberrantly dividing cells.

Accumulating evidence from genetic knockouts of the CDKs and/or their cyclin partners and from siRNA studies suggests significant redundancy in their regulation of key cell cycle events.^{28–32} In addition, the effects of CDK inhibitors on cell proliferation and the induction of apoptosis are not fully reconciled with the current understanding of the biological functions of individual CDKs and the CDK family as a whole. Therefore, an inhibitor active against more than one of the key CDKs may have additional benefits in terms of antitumor activity.

Not surprisingly, with the wealth of underlying biological rationale, the development of chemical modulators of CDKs as new anticancer agents has engendered significant interest, with several compounds in clinical and preclinical development.^{33,34}

First generation CDK inhibitors such as **1** (Flavopiridol/L868275)³⁵ and 7-hydroxystaurosporine³⁶ (UCN-01) have been evaluated in the clinic for some time, and recently **1** has been granted orphan drug status for the treatment of chronic lymphocytic leukemia.³⁷ Inhibitors with greater selectivity for the CDKs such as **2** (roscovitine/CYC-202),³⁸ **3** (BMS-387032/SNS-032)³⁹ (both primarily target CDK2, but also possess significant CDK7 and 9 activity), and **4** (PD0332991)⁴⁰ (a selective CDK4/6 inhibitor) (Figure 1) are currently being evaluated in phase I and II clinical trials, but limited results have been published to date.

Hit Identification. Apo crystals of CDK2 were soaked with cocktails of targeted fragments (4 fragments per cocktail). The screening set of about 500 compounds was made up from a focused kinase set, a drug fragment set, and compounds identified by virtual screening against the crystal structure of CDK2.¹ Multiple (>30) low-affinity fragment hits were identified that bind in the adenosine 5'-triphosphate (ATP) binding

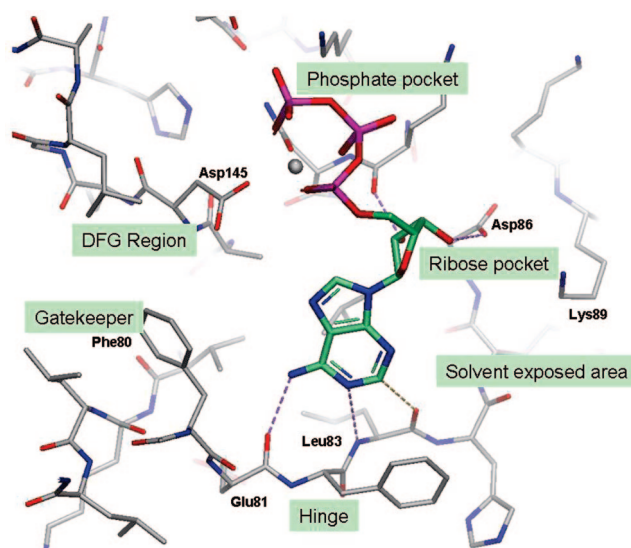


Figure 2. X-ray crystal structure of ATP (adenosine triphosphate) bound into the active site of CDK2 (1HCL). The ligand is anchored in place with two hydrogen bonds, one between the backbone carbonyl of Glu81 and the 6-amino group and one between the backbone NH of Leu83 and the N1 position of the adenine ring. An additional favorable electrostatic interaction is made between the hydrogen atom at the C2 position and the carbonyl of Leu83. The ribose and phosphate groups form multiple polar interactions, one of which involves coordination to the catalytic magnesium (gray/silver sphere) via the phosphate groups along with Asp145 and Asn132. Other key features to notice are that ATP does not interact with the solvent accessible region or the hydrophobic pocket between the gatekeeper residue and the DFG region.

site. A conserved structural feature of all the bound fragments was one or more hydrogen bonding interactions to key backbone residues at the hinge region of CDK2 (Glu81 and Leu83). ATP itself adopts a similar binding mode, as illustrated in Figure 2.⁴¹ The compounds shown in Figure 3 are a representative selection of the hits identified during fragment screening (compounds **5–8**). The hits had only low potency (40 μ M to 1 mM) but were highly efficient binders given their low molecular weight (<225) and limited functionality. An important consideration during our fragments-to-leads phase is pursuing multiple series in parallel in order to have two or more series for optimization in the later stages of the project. A key feature of this process was the collection of multiple protein–ligand crystal structures to guide iterative cycles of optimization.^{1,2}

To enable the design process, a detailed analysis of the ATP binding site of CDK2 and binding mode of known CDK inhibitors was carried out. The analysis identified a number of key interactions and regions of the protein to target in order to optimize activity and physicochemical properties (Figure 2). Hydrogen bonds to the backbone carbonyl and NH of Leu83 and the backbone carbonyl of Glu81 were commonly observed with bound fragments and more potent ligands. Making all three of these interactions with the hinge appeared to be a potential way to design a very potent and ligand efficient inhibitor. Other key areas to explore included the relatively small region between the gatekeeper residue (Phe80) and the catalytic aspartic acid (Asp145) of the DFG motif and a hydrophobic pocket leading to the solvent exposed region (defined by Phe82, Ile10, Leu134, and side chain methylene of Asp86). A number of inhibitors in the literature appeared to interact with Asp86, and this was targeted with some early compounds.^{42,43} The solvent accessible region toward Lys89 was identified as potentially suitable for modulating physicochemical properties, particularly for increas-

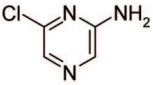
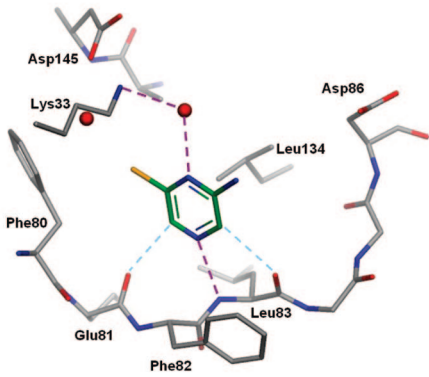
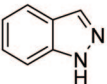
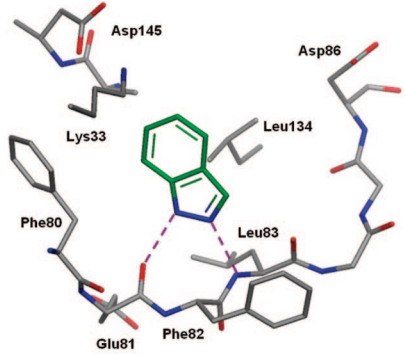
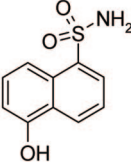
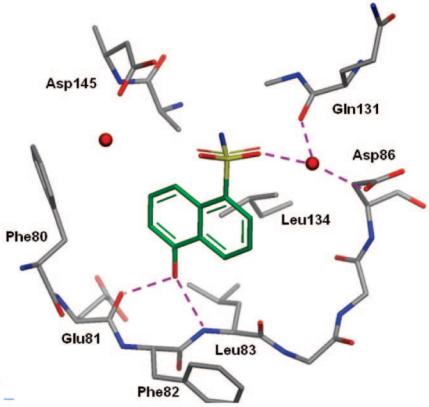
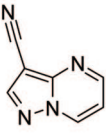
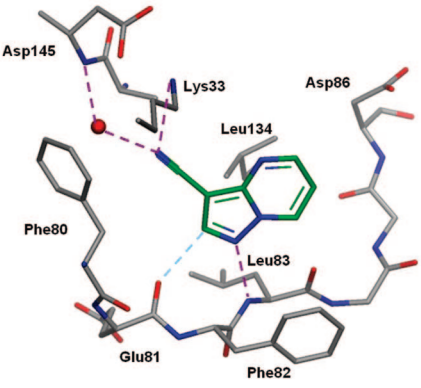
Ligand	Protein-Ligand Complex	Description of the binding mode
 <p>5</p> <p>MW = 130 %I = 64% at 1 mM LE < 0.51</p>		<p>Fragment 5 forms only one classical hydrogen bond with the protein, between the nitrogen at the 4-position and the amide NH of Leu83. The adjacent aromatic C-H's on the pyrimidine form favorable electrostatic interactions (blue dotted lines) with the backbone carbonyl oxygen's of Leu83 and Glu81. The fragment forms additional hydrophobic interactions with the side chains of Ile10, Val18, Ala31 (not shown), Phe80, Phe82 and Leu134 which form the sides of the relatively narrow binding cleft.</p>
 <p>6</p> <p>MW = 118 IC₅₀ = 185 μM LE = 0.57</p>		<p>Indazole 6 forms two classical hydrogen bonds acting as both a donor and an acceptor to the backbone carbonyl of Glu81 and the NH of Leu83. This fragment also forms similar hydrophobic contacts to 5.</p>
 <p>7</p> <p>MW = 223 IC₅₀ = 120 μM LE = 0.36</p>		<p>The naphthol OH forms a bidentate interaction with the backbone carbonyl of Glu81 and the NH of Leu83. The sulphonamide moiety forms water mediated hydrogen bonds to the backbone carbonyl of Gln131 and to the side chain carbonyl of Asp86, partly occupying the ribose pocket (see Figure 2). The hydrophobic core of the fragment forms lipophilic contacts with Ile10, Val18, Ala31 (not shown), Phe80, Phe82 and Leu134.</p>
 <p>8</p> <p>MW = 144 %I = 54% at 1 mM LE < 0.37</p>		<p>The key hydrogen bonding interaction is between the N1 of the pyrazolopyrimidine and the backbone NH of Leu83. The two adjacent aromatic C-H's (at the 2 and 7 positions) form positive electrostatic interactions with the backbone carbonyls of Glu81 and Leu83. The nitrile group appears to interact with the aromatic π system of Phe80, whilst forming hydrogen bonds with the backbone NH of Asp145 (through a conserved water molecule) and to the side chain of Lys33. 8 forms similar hydrophobic contacts to the previous examples.</p>

Figure 3. Fragment–protein cocomplexes of four low-molecular-weight hits identified by fragment-based X-ray crystallographic screening (**5–8**). On the left is shown the fragment structure and available IC₅₀ data, in the center a pictorial representation of the protein–ligand complex, and the right-hand column provides a description of the experimentally determined binding mode. Key: red spheres, water molecules; purple dashed lines, protein–ligand and water–ligand hydrogen bonds; blue dashed lines, other electrostatic interactions. The PDB code for compound **5** is 1WCC.

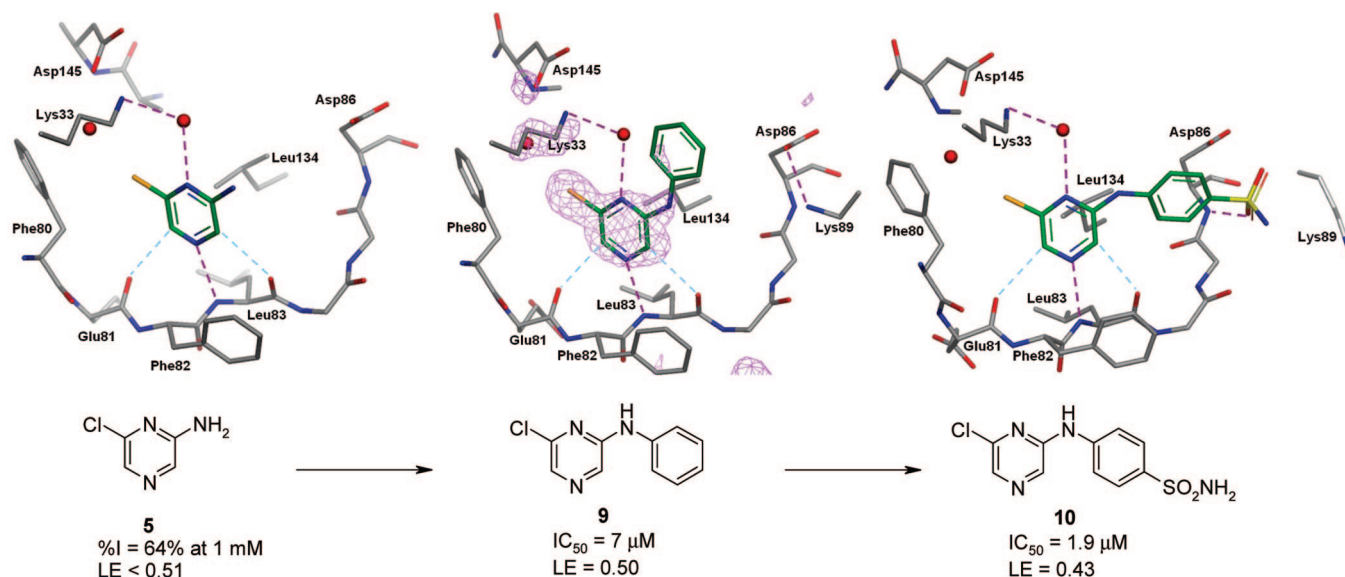


Figure 4. Fragment to lead optimization of pyrazine-based inhibitors. Compound **5** possesses reasonable growth points toward the gatekeeper residue (Phe80) and from the amino group out toward the solvent exposed region. Hydrophobic space filling by substitution at the 2-amino position with an aryl group gave compound **9** (7 μM; LE = 0.50), displaying a 150-fold jump in activity over the starting fragment **5**. Perhaps surprisingly, the structural data quality for this compound was poor, with no electron density observed for the aryl group, possibly due to the aryl group being able to bind in a number of conformations. Introduction of a sulfonamide at the 4-position of the aryl group forces an intramolecular salt bridge between Asp86 and Lys89 to break and allows for the formation of a further H-bonding interaction between the sulfonamide and the backbone NH of Asp86. In spite of this additional interaction, only a modest increase in activity is observed for **10** (1.9 μM; LE = 0.43).⁵¹ Further modification of this group or replacement of the 6-chloro substituent suggested that optimization beyond low micromolar activity was not straightforward, so this series was not pursued further. Key: red spheres, water molecules; purple dashed lines, protein–ligand and water–ligand hydrogen bonds; blue dashed lines, other electrostatic interactions.

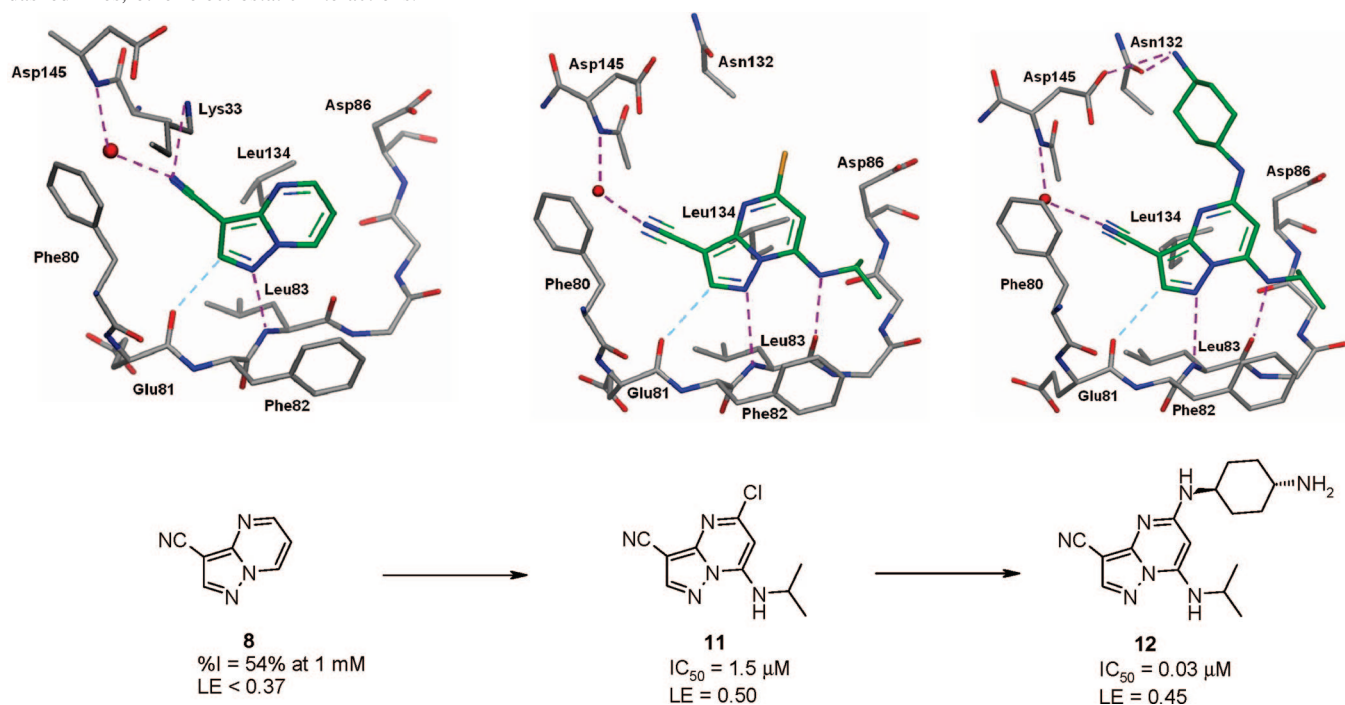


Figure 5. Fragment to lead optimization of pyrazolopyrimidine-based inhibitors. Fragment **8** binds to CDK2 as described in Figure 3. The binding mode is very similar to that of Roscovitine (**2**) and other bicyclic templates described in the literature. Substitution of compound **8** at the 7-position with a hydrogen bond donor allowed a third interaction to be formed with the protein backbone at the hinge region (carbonyl of Leu83). The amine could be substituted with a range of functionalities and the isopropyl group being particularly effective. Compound **11** gave a 700-fold jump in binding affinity (IC₅₀ = 1.5 μM, LE = 0.50) and an improvement in ligand efficiency over the starting fragment. Growing out from the 5-position allowed the opportunity to access the ribose and phosphate binding regions of the active site. Introduction of basic functionality in the phosphate binding pocket was well tolerated, with this strategy producing the high affinity lead **12** (IC₅₀ = 0.03 μM, LE = 0.45). The crystal structure shows the 4-amino group to be forming hydrogen bonds with the carboxylate of Asp145 and the side chain carbonyl of Asn132, mimicking the Mg²⁺ observed in many ATP bound kinase complexes. Compound **12** also displayed good cellular activity (HCT116 cell IC₅₀ = 0.29 μM), however, this did not translate into in vivo activity and work on this series was abandoned in favor of more promising compounds. Key: red spheres, water molecules; purple dashed lines, protein–ligand and water–ligand hydrogen bonds; blue dashed lines, other electrostatic interactions.

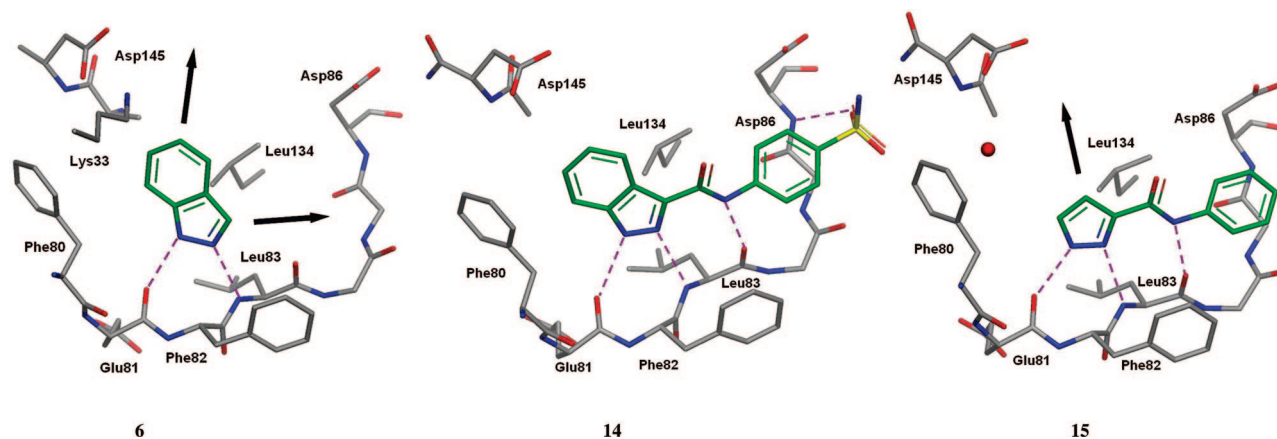


Figure 6. CDK2 cocrystal structures of compounds **6**, **14**, and **15**. Key: red spheres, water molecules; purple dashed lines, protein–ligand hydrogen bonds; arrows indicate potential vectors for substitution.

ing water solubility. Many of these interactions are discussed in an interesting review by Liao on the molecular recognition of protein kinase binding pockets.⁴⁴

Results and Discussion

Summary of Fragment to Lead Optimization. Figure 3 shows four representative fragment hits identified by structural screening of CDK2. A number of considerations were taken into account when deciding which of the hits should be worked on further, and these included LE, vectors suitable to access the key regions highlighted in Figure 2, novelty, and synthetic tractability. Of the fragments described, compound **7** was assessed not to have suitable vectors for optimization and, in addition, the chemistry did not appear to be very tractable. As a result, this compound did not enter hit-to-lead chemistry. Compounds **5**, **6**, and **8** were deemed to have suitable vectors and the chemistry sufficiently tractable to warrant further work. The optimization of compounds **5** and **8** is outlined in brief in Figures 4 and 5, respectively; the optimization of compound **6** will be discussed in detail in the following sections.

Fragment to Lead Optimization of Compound 6. The “hit to lead” chemistry of **6** focused primarily on two vectors (from the 3 and 5 positions of the indazole ring, see Figure 6) suitable to access pockets identified by the kinase structural analysis (Figure 2). Structural data from Astex fragments and known CDK inhibitors suggested that formation of an additional hydrogen bonding interaction to the carbonyl of Leu83 was a possibility.^{45,46} This was achieved by linking an aryl amide to the 3-position of indazole, resulting in **13** ($IC_{50} = 3 \mu M$; LE = 0.42) (Table 1). The phenyl ring was twisted out of plane and occupies the hydrophobic pocket formed by the backbone of the linker region and side chains of Ile10 and Leu134. Addition of a sulfonamide group at the 4-position of the phenyl ring afforded **14** with submicromolar activity ($IC_{50} = 0.66 \mu M$; LE = 0.38). The sulfonamide picks up two further interactions, both to Asp86, a direct hydrogen bond to the backbone NH and a water-mediated interaction to the carboxylate side chain (Figure 6).^{42,43}

Substitution of the indazole ring at the 4 or 5 positions resulted in relatively small increases in CDK2 activity, while as expected, substitutions at the 6 or 7 positions were poorly tolerated (data not shown) due to the close proximity of Phe80.

An alternative strategy was pursued in parallel and rather than seeking to increase the potency of **14** by continuing to add molecular weight, the system was simplified by removal of the fused benzene ring to afford the pyrazole **15** ($IC_{50} = 97 \mu M$;

Table 1. CDK2 Inhibition of Selected Indazole and Pyrazole Amides^a

Compound	Structure	CDK2 ^b	
		IC_{50} / % I (μM)	LE
13		3	0.42
14		0.66	0.38
15		97	0.39
16		25	0.45
17		85	0.35
18		0.85	0.44
2^b	-	0.37	0.34

^a Compound were assayed 2 or more times. ^b IC_{50} data for **2** was generated in house and compares well with values quoted in the literature (within 2 fold).⁴⁷

LE = 0.39). Despite a drop in activity, the LE was similar to the more elaborated compounds and the binding mode as

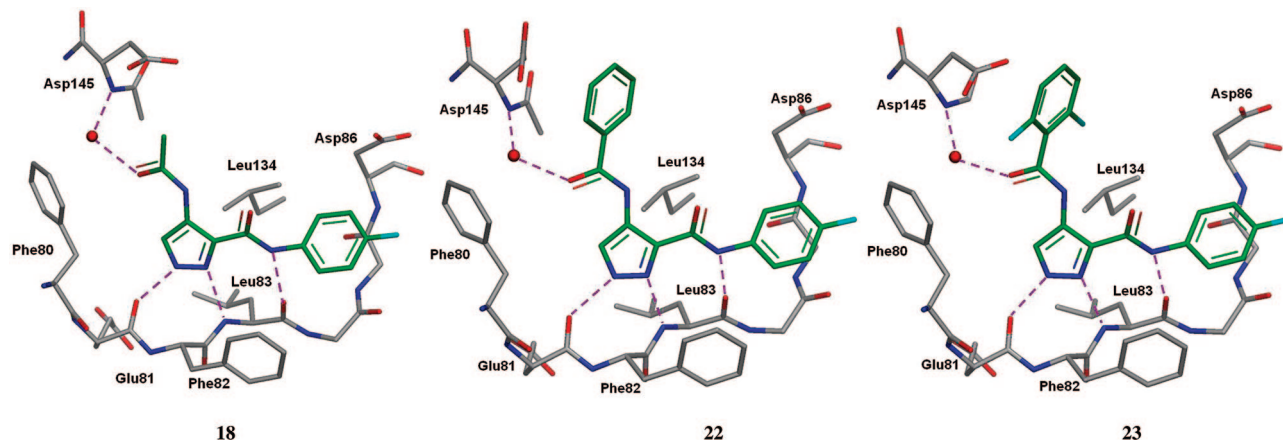


Figure 7. CDK2 cocrystal structures of compounds **18**, **22**, and **23**, demonstrating the use of 2,6-disubstitution on the phenyl ring (**23**) to stabilize the induced twist observed for the benzamide of **22** on binding to CDK2. Key: red spheres, water molecules; purple dashed lines, protein–ligand and water–ligand hydrogen bonds.

confirmed by the X-ray crystal structure remained identical to the starting fragment, which encouraged us to pursue this strategy further. The change of hinge binder provided a significantly different vector and improved access to the DFG region between the gatekeeper residue (Phe80) and the catalytic aspartate (Asp145) (Figure 2). It appeared that derivatizing the pyrazole at the 4-position presented an opportunity to grow into this pocket (Figure 6). Accordingly, introduction of a 4-amino group as a synthetic handle gave **17** which resulted in a modest increase in activity ($IC_{50} = 85 \mu\text{M}$; $LE = 0.35$). Introduction of a hydrogen bond acceptor gave compounds such as the amide **18**, leading to a 100-fold increase in activity and improved LE ($IC_{50} = 0.85 \mu\text{M}$; $LE = 0.44$). An X-ray structure of **18** bound into CDK2 showed that the increase in activity was at least in part due to a water mediated hydrogen bond from the acetamide carbonyl oxygen to the backbone NH of Asp145 (Figure 7). Another important observation is that the planarity of **18** is achieved due to an intramolecular hydrogen bond between the acetamide NH and the benzamide carbonyl, allowing the compound to fit into the narrow binding pocket.

Ongoing with this work were attempts to replace the amide at the 3-position of the pyrazole with alternative groups that could maintain the hydrogen bonding interaction to the backbone carbonyl of Leu83 while maintaining the planarity of the system. For example, a 2-benzimidazole group proved to be an effective replacement for the aryl amide. **16** ($IC_{50} = 25 \mu\text{M}$; $LE = 0.45$) is more active than the corresponding amide **15**. Further optimization of **16** led to the identification of an alternative series with excellent kinase and cell activity. Details of the development of this alternative series will follow in a subsequent publication.

The protein–ligand structure of **18** indicated that the methyl of the acetamide group is in very close proximity to the side chain carboxylate of Asp145 (approximately 3.5 Å), making the pocket relatively small. Some protein flexibility is observed in this region of the binding site, so in order to probe this area further, a limited number of amides with diverse properties were synthesized (Table 2). A range of simple functionalities such as **19** and **20** did not afford a significant increase in activity over **18**; however, interesting levels of kinase activity were obtained with directly attached monocycles such as the cyclohexyl amide **21** and benzamide **22**, and these compounds also showed some indication of cellular activity. The benzamide **22** was particularly interesting, showing only a small increase in binding affinity and a decrease in ligand efficiency ($IC_{50} = 0.14$

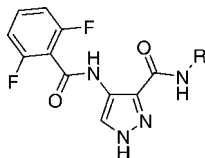
Table 2. Pyrazole Diamide Structure–Activity Relationships (SAR)

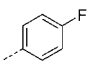
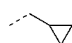
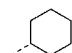
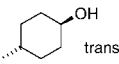
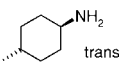
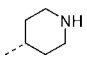
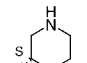
Compound	R	CDK2 ^a		HCT116 ^a
		IC_{50} (μM)	LE	IC_{50} (μM)
19		0.73	0.42	33*
20		1.6	0.32	ND
21		0.09	0.40	3.4
22		0.14	0.39	3.9
23		0.003	0.45	1.4

^a Compounds were assayed 2 or more times unless indicated * where $n = 1$.

μM , $LE = 0.39$); however, the protein–ligand crystal structure (Figure 7) provided a number of important insights into the binding mode of this compound. First, a small amount of protein movement had occurred, allowing the aromatic ring to be accommodated. Second the phenyl ring was significantly twisted out of plane of the amide, with a torsion angle of 51° , an energetically unfavorable conformation. It was postulated that stabilization of this twist by diortho substitution of the phenyl ring might be beneficial. The X-ray structure confirmed that **23** bound to CDK2 as predicted (Figure 7), resulting in a 45-fold increase in kinase activity for the addition of only two heavy atoms and with a ligand efficiency very similar to the starting fragment ($IC_{50} = 0.003 \mu\text{M}$, $LE = 0.45$).

Although **23** exhibited good kinase activity and its pharmacokinetic (PK) properties indicated it to be a good lead molecule,

Table 3. Summary of SAR for Compounds **23**–**29**


Compound	R	CDK1 ^a IC ₅₀ (μM)	CDK2 ^a IC ₅₀ (μM)	HCT116 ^a IC ₅₀ (μM)	Plasma clearance ^b ml/min/kg
23		0.010	0.003	1.4	40
24		-	0.025	2.1 [*]	66
25		0.055	0.012	0.55	65
26		0.045	0.019	0.32	42
27		0.44	0.038	0.25	63
28		0.98	0.14	0.31	43
29		0.038	0.044	0.13	48

^a Compounds were assayed 2 or more times unless indicated * where $n = 1$. ^b The plasma clearance data was determined after IV administration to BALB/c mice at 0.2 mg/kg according to Pharmacokinetic Study Methods.

with moderate plasma clearance (40 mL/min/kg) after intravenous (iv) dosing in mice, its antiproliferative cell activity against HCT116 colon cancer cells was only moderate (1.4 μM). One explanation for this moderate cell activity may be due to low cell permeability. **23** has a ClogP of 2.4, however, the measured value is approximately 2 log units higher, presumably due to internal hydrogen bonding reducing the overall polarity of the molecule. This relatively high lipophilicity may be detrimental to cell permeability, and in an attempt to address this, further optimization of the series was sought by replacing the lipophilic 4-fluorophenyl group of **23** (Table 3). In general, other aromatic groups (data not shown) and simple alkyl groups such as in **24** gave good kinase activity but only moderate cell activity. However, the directly attached cycloalkyl ring of **25** gave an improvement in kinase activity and was the first compound in this series with submicromolar cell activity. Because of its reasonable cellular activity the PK properties of **25** were determined in mice and it was found to have high plasma clearance (65 mL/min/kg). A potential cause of this was oxidative metabolism of the highly lipophilic cyclohexyl group, and in an attempt to address this, modifications were made to the cyclohexyl ring. Although a number of 4-substituted cyclohexyl derivatives such as **26** and **27** exhibited good kinase and cell activity, most had relatively high plasma clearances. Introduction of a nitrogen atom into the ring affording **28** and **29** gave compounds with good CDK2 and cell potency. It became apparent from making these small polar changes that modulating physicochemical properties was just as important as increasing kinase activity when attempting to improve cell potency. Interestingly, the 3-piperidinyl isomer **29** exhibited an

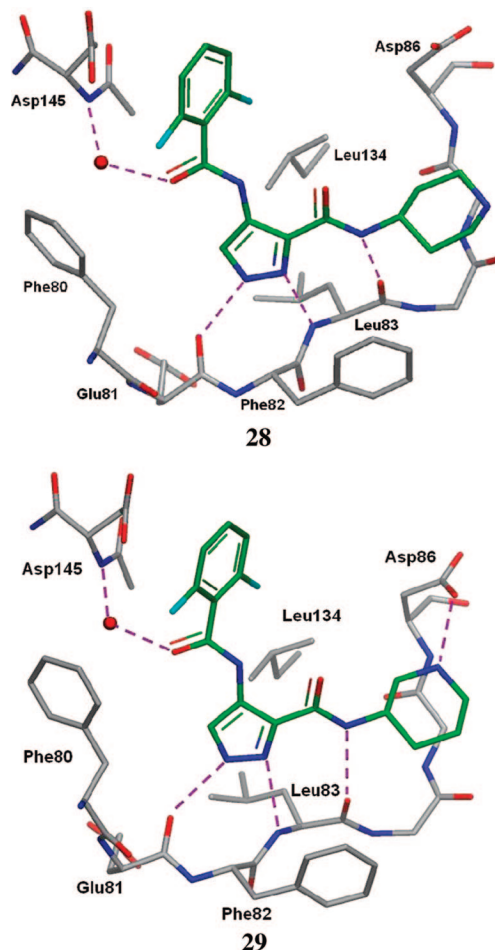
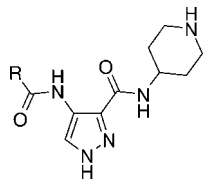
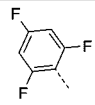
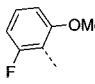
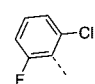
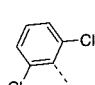


Figure 8. CDK2 cocrystal structures of compounds **28** and **29**. **29** forms an additional hydrogen bond between the ring nitrogen of the piperidyl group and the carboxylate of Asp86. This may explain the observed improvement in binding affinity. Key: red spheres, water molecules; purple dashed lines, protein–ligand and water–ligand hydrogen bonds.

increase in CDK1 as well as CDK2 activity compared to **28**. This increase in activity can be explained by the presence of a conserved carboxylate residue in CDK1 and CDK2 (Asp86 in CDK2) with which the 3-piperidinyl nitrogen of **29** can interact. The X-ray structure of **29** bound to CDK2 (Figure 8) confirms this interaction, the protonated nitrogen being 2.65 Å from the carboxylate of Asp86. Compound **28** was considered to be a promising lead due to its reasonable cell activity and acceptable plasma protein binding (PPB) (Table 5); as a consequence of this, further in vivo characterization of **28** was performed. Despite showing moderate plasma clearance (43 mL/min/kg), the compound was dosed to mice bearing HCT116 tumor xenografts to determine the level of compound in the tumor. After a single 10 mg/kg dose of **28** was administered via the ip route, reasonable, albeit somewhat variable levels of compound appeared to distribute into tumor (AUC = 3422 ± 2478 h·ng/g) (Table 5). The compound was much more rapidly cleared from plasma, with negligible material remaining after 7 h (data not shown). In an attempt to determine whether compound levels in tumor were a potential indicator of in vivo efficacy, **28** was evaluated for antitumor activity in a mouse xenograft model. The hydrochloride salt of compound **28** was dosed ip bid (twice daily) at 18.2, 9.1, and 4.6 mg/kg to SCID mice bearing early stage HCT116 human colon carcinoma xenografts for 10 days. Compound **28** showed a clear dose–response for antitumor

Table 4. Substituted Benzamide SAR for Compounds **30**–**33**


Compound	R	CDK2 ^a	HCT116 ^a	Plasma clearance ^b
		IC ₅₀ (μM)	IC ₅₀ (μM)	ml/min/kg
30		0.75	0.91	71
31		0.035	0.052	38
32		0.11	0.063	56
33		0.047	0.082	52

^a Compounds were assayed 2 or more times. ^b The plasma clearance data was determined after IV administration to BALB/c mice at 0.2 mg/kg according to Pharmacokinetic Study Methods.

activity although the dose schedule was not optimized. The 18.2 mg/kg dose group showed tumor growth inhibition of 86% (%T/C = 14), however this dose was not well tolerated. At a tolerated dose of 9.1 mg/kg, growth inhibition was 46% (%T/C = 54) (Table 5) and the 4.6 mg/kg group showed 22% growth inhibition (%T/C = 78). These data suggested that distribution of compounds in tumor and their persistence there might be a useful indicator of in vivo activity when considered alongside protein binding and cell potency. The further impact of compound disposition on biomarker modulation will be discussed in a subsequent paper.

Further optimization of **28** aimed at increasing activity against CDK2 and subsequently improve cell activity was explored by reoptimizing the 2,6-difluorophenyl moiety (Table 4). Attempts to block potential metabolism of the phenyl ring by substitution of the 4-position, e.g., in **30** resulted in somewhat reduced inhibitory activity against the kinase. Replacement of one of the fluorines of **28** with small substituents such as methoxy and chloro to give **31** and **32** was well tolerated and resulted in increased kinase and cell activity (Table 4). The 2,6-dichlorophenyl derivative **33** gave an increase in kinase and cell activity, as the chlorine atoms filled this lipophilic pocket more

effectively than fluorine. Because previous compounds showed persistence in tumor in spite of moderate to high plasma clearance (e.g., **28**), further compounds (**31** and **33**) were dosed to HCT116 tumor bearing mice at 10 mg/kg to determine tumor distribution properties. A similar trend to compound **28** was observed, with significant levels of both **31** and **33** present in tumor (AUC = 3325 ± 543 and 6260–6340 h·ng/g, respectively) (Table 5). Compound **33** in particular showed good tumor exposure.

The promising in vitro kinase and antiproliferative cell activity, coupled with low PPB and reasonable tumor distribution for both **31** and **33**, led them to be evaluated in vivo for potential antitumor efficacy. Compound **31** showed 38% tumor growth inhibition (%T/C = 62) in the HCT116 mouse xenograft model at 10 mg/kg, although the dose and schedule were not optimized. Compound **33** showed significant efficacy in the same tumor type producing tumor growth inhibition of 87% (%T/C = 13) when dosed at 9.1 mg/kg ip bid for 10 days (Table 5), which warranted further investigation. A similar beneficial effect was observed for **33** in the A2780 (human ovarian carcinoma cell line) mouse xenograft model. Details of this and further characterization of **33** is described in the following section.

Characterization of Compound 33. Kinase Selectivity Profile. Compound **33** was profiled more widely against a panel of kinases (see Supporting Information). In addition to CDKs 1 and 2 (IC₅₀s 190 nM and 47 nM, respectively), **33** potently inhibited a number of other CDKs (4 and 5 in particular, IC₅₀s 67 nM and 18 nM, respectively), but had lower activity against other kinases tested (more detailed selectivity data will be published in a subsequent paper). One explanation for the observed selectivity over some kinases (Aurora A, IR kinase, MEK, PDK1, c-abl, IC₅₀ > 10 μM) is shown in Figure 9a. All these kinases possess an additional glycine residue (in between the amino acids corresponding to Gln85 and Asp86 of CDK2), which causes the main chain to bulge into the ATP binding pocket resulting in a clash with the piperidine of **33**.

Cell-Based Activity. Compound **33** is a potent inhibitor of HCT116 cell proliferation (used as a primary screen during lead optimization). Following 72 h exposure, **33** potently inhibited the proliferation of a range of human tumor cell lines (over 100 cell lines have been tested), with compound **33** showing sub 1 μM activity against more than 75 (data not shown). Compound **33** had reduced antiproliferative activity against the nontransformed fibroblast cell line, MRC-5, but more significantly, it did not affect the viability of noncycling MRC-5 cells at doses up to 10 μM (Table 6). These data suggest that the antiproliferative activity is cell cycle related and not due to general cytotoxicity to nondividing cells.

The mechanism of action of **33** in cells was investigated by monitoring the phosphorylation state of substrates specific for the various CDKs, following treatment with **33** for 24 h. These studies indicated that inhibition of phosphorylation of the CDK1 substrate PP1α (Thr320) and the CDK2 substrates Rb (Thr821) and Nucleophosmin (NPM) (Thr199) (data to be published in

Table 5. Activity, Distribution, and Initial Efficacy Parameters for Compounds **28**, **31**, and **33**

Compound	HCT116 ^a IC ₅₀ (μM)	Plasma protein binding (% bound)	Tumor AUC _(0-t) h·ng/g ^b	Efficacy screening protocol in HCT116 tumor xenograft model	% T/C ^c
28	0.31	84	3422 ± 2478 (n = 4)	9.1 mg/kg/dose bid QDx10 ^c	54
31	0.052	75	3325 ± 543 (n = 3)	10 mg/kg/dose bid QDx9 ^d	62
33	0.082	42	6260–6340	9.1 mg/kg/dose bid QDx10 ^c	13

^a Compounds were assayed 2 or more times. ^b Mean ± SD for n determinations or range for n = 2 determinations. ^c Efficacy study conducted in SCID mice following ip administration. ^d Efficacy study conducted in BALB/c nude mice following ip administration. ^e %T/C is the mean tumor volume of treated animals divided by the mean control tumor volume expressed as a percentage.

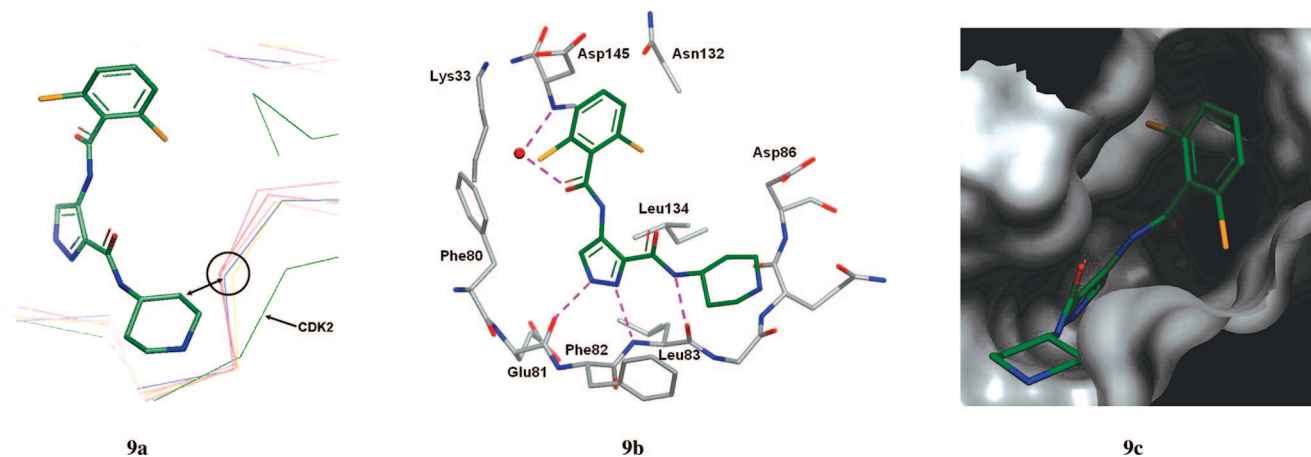


Figure 9. (a) Overlay of C- α traces of the crystal structure of **33** bound into CDK2 (green) with the crystal structures of Aurora A (PDB code 1OL6, yellow), insulin receptor (IR) kinase (1GAG, brown), MEK1 (1S9J, purple), PDK1 (1UU3, blue), and c-abl (1IEP, red), showing the clash of the kinases (except CDK2) with the piperidine of **33**. Aurora A, IR kinase, MEK1, PDK1, and c-abl all have IC_{50} values $> 10 \mu M$. (b) CDK2 cocrystal structures of compound **33**. Key: red spheres, water molecules; purple dashed lines, protein-ligand and water-ligand hydrogen bonds. (c) Molecular surface representation of CDK2 with **33** bound in the ATP binding site. The piperidine moiety is pointing out of the pocket toward solvent. The twisted 2,6-dichlorophenyl is toward the back of the pocket, with the two chlorine atoms efficiently filling small hydrophobic pockets.

Table 6. In Vitro Antiproliferative Activity of **33** in a Panel of Human Tumor Cell Lines

Origin	Cell line	IC_{50} (nM)
colon carcinoma	HCT116	82
ovarian carcinoma	A2780	350
fibroblast	MRC 5	980
	MRC 5 (nonproliferative)	> 10000

Table 7. Mouse PK Data of Compound **33** after iv Administration to BALB/c Mice^a

$t_{1/2}$ (h)	Cl (ml/min/kg)	V_{ss} (L/kg)
0.68 ± 0.28	46 ± 21	1.6 ± 0.9

^a Mean \pm SD for $n = 5-7$ replicate studies.

a subsequent paper) in HCT116 cells occurred at doses consistent with the observed antiproliferative effects.

Pharmacokinetics Study. As summarized in Table 7, the systemic clearance of **33** in BALB/c mice after iv dosing averaged 46 mL/min/kg with a mean half-life ($t_{1/2}$) and volume of distribution (V_{ss}) of 0.68 h and 1.6 L/kg, respectively. **33** showed low oral bioavailability ($< 1\%$), which was a common feature of many closely related basic compounds.

In Vivo Antitumor Activity. Compound **33** was evaluated for its in vivo antitumor activity in nude BALB/c mice bearing early stage A2780 human ovarian carcinoma xenografts with a mean starting volume of approximately 50 mm³ (Figure 10). In this study, the hydrochloride salt of **33**, dissolved in 0.9% saline, was administered by the intraperitoneal (ip) route, twice daily, for 8 consecutive days. Tumor growth inhibition at the end of the experiment was 86% at the 7.5 mg/kg dose level (%T/C = 14). A more extensive biological characterization of compound **33**, including a comprehensive cell cycle analysis and a detailed in vivo efficacy evaluation will be published separately.

Chemistry. Compounds **13**, **14**, and **15** were synthesized by coupling either 1*H*-indazole-3-carboxylic acid or 1*H*-pyrazole-3-carboxylic acid with aniline or 4-aminobenzenesulfonamide. Compound **16** was prepared by coupling 1*H*-pyrazole-3-carboxylic acid with 1,2-diaminobenzene followed by acid mediated cyclization to form the benzimidazole. Synthesis of aminopyrazole **17** was achieved (Scheme 1) by coupling

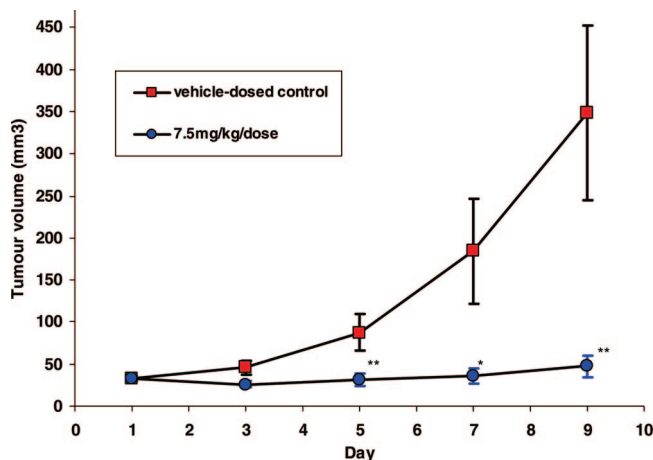
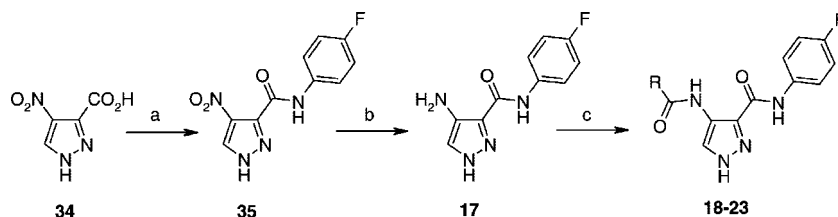


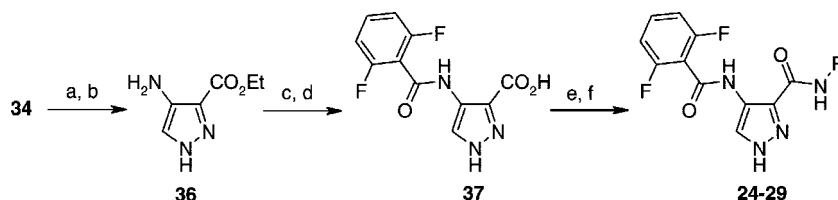
Figure 10. Efficacy of **33** in the early stage A2780 ovarian carcinoma xenograft mouse model following repeated administration at 7.5 mg/kg/dose given twice daily by the intraperitoneal route for 8 days against a matched vehicle-dosed control. Tumor growth curves \pm SE for groups of $n = 12$. Growth curves became significantly different from control from day 5 onward (* $p < 0.05$, ** $p < 0.001$). The CDK2 and cellular IC_{50} data quoted is the mean based on a minimum of two separate determinations.

4-nitropyrazole-3-carboxylic acid **34** with 4-fluoroaniline, followed by catalytic hydrogenation of **35** with palladium on carbon. Diamides **18-23** were synthesized by coupling of **17** with acetic anhydride or the appropriate carboxylic acids using EDC/HOBt.

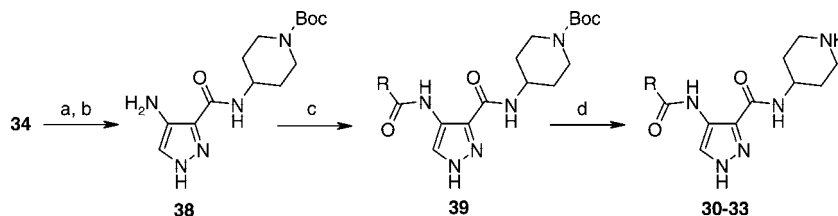
Esterification of **34** with ethanol under acidic conditions followed by catalytic hydrogenation of the nitro group gave the aminopyrazole **36** (Scheme 2). Acylation of **36** with 2,6-difluorobenzoic acid, followed by basic hydrolysis afforded pyrazole acid **37**. Coupling of **37** with the required amines using EDC/HOBt gave compounds **24-26**. Compounds **27-29** required an additional deprotection step to remove the *N*-*tert*-butoxycarbonyl group. This was achieved under standard acidic conditions with saturated HCl in EtOAc. The piperidine amides **30-33** were synthesized via the aminopyrazole **38** (Scheme 3), itself synthesized from the coupling of 4-amino-piperidine-1-carboxylic acid *tert*-butyl ester and **34**, followed by reduction of the nitro group. Coupling of **38** with the appropriate

Scheme 1^a

^a Reagents and conditions: (a) 4-fluoroaniline, EDC, HOBt, DMF; (b) 10% Pd/C, EtOH, H₂; (c) Ac₂O, pyridine, or RCO₂H, EDC, HOBt, DMF, or DMSO.

Scheme 2^a

^a Reagents and conditions: (a) SOCl₂, EtOH; (b) 10% Pd/C, EtOH, H₂; (c) 2,6-difluorobenzoic acid, EDC, HOBt, DMF; (d) NaOH, MeOH/H₂O (1:1); (e) RNH₂, EDC, HOBt, or HOAt, DMF, or DMSO; (f) saturated solution of HCl in EtOAc (where R contains a Boc protected amine).

Scheme 3^a

^a Reagents and conditions: (a) 4-amino-piperidine-1-carboxylic acid tert-butyl ester, EDC, HOBt, DMF; (b) 10% Pd/C, EtOH, H₂; (c) RCO₂H, EDC, DMF; (d) saturated solution of HCl in EtOAc.

carboxylic acids, then acidic deprotection of the Boc protected piperidine of **39**, afforded compounds **30–33**. During preclinical development, compound **33** was synthesized by a six-step route (similar to Scheme 2) in multikilogram quantities with an overall yield of 80% and purity >99%, without the requirement for purification by column chromatography.

Conclusions

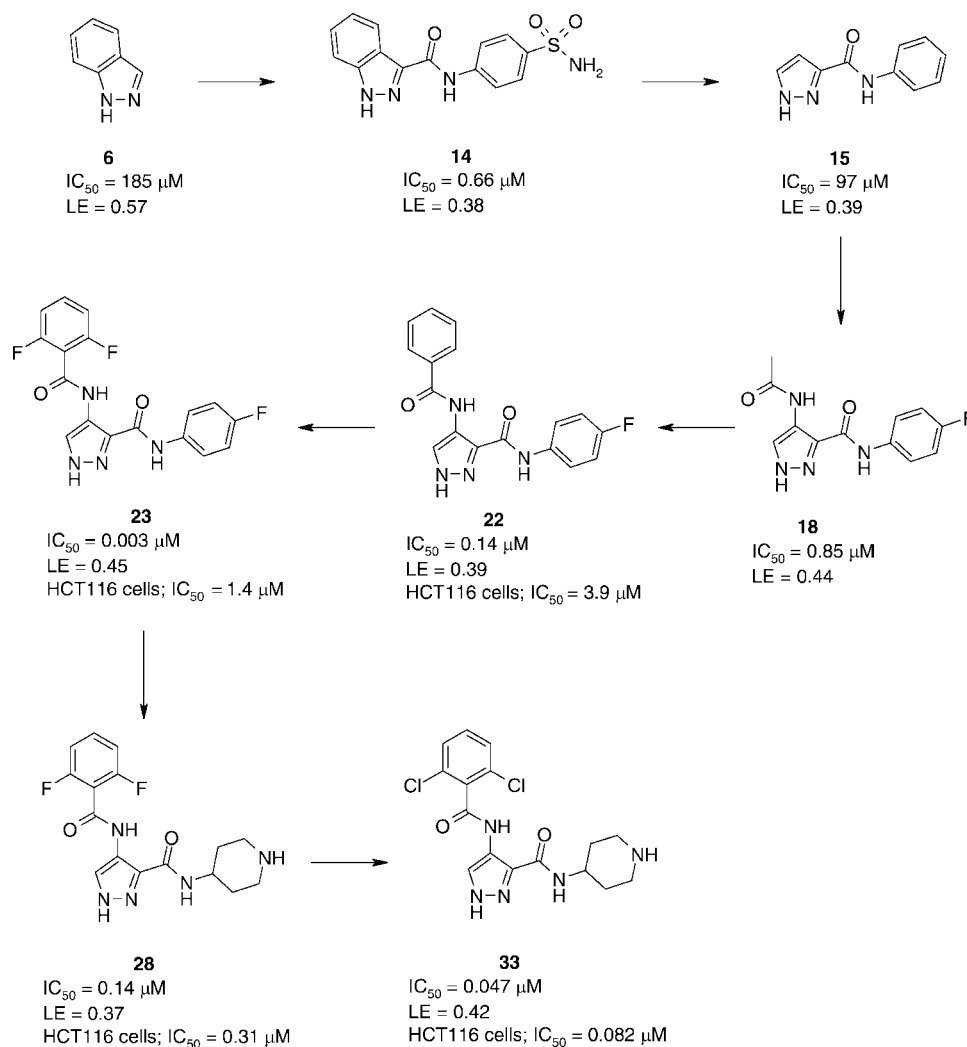
High-throughput X-ray crystallographic screening of fragment libraries was used to identify multiple hits that bound to CDK2. A number of these fragment hits were elaborated in parallel with the aid of detailed structural information enabling the project to take 3 series into late stage lead optimization. Optimization of the indazole hit **6** eventually led to the discovery of AT7519 (**33**). The key compounds in the discovery of **33** are summarized in Scheme 4. Important structural features identified throughout the optimization process include (Figure 9b): (i) a donor–acceptor–donor interaction anchoring the molecule to the hinge region of CDK2 (residues Glu81 and Leu83), (ii) a water mediated hydrogen bond between the carbonyl of the 4-benzamide group and the backbone N–H of Asp145, (iii) stabilization of the twisted benzamide conformation by introduction of two ortho-substituents, (iv) introduction of the solubilizing aminopiperidine amide group resulted in improved hydrophobic filling of the region bounded by the backbone of the hinge and sidechains of residues Phe82, Ile10, Leu134, and Asp86 and which led to selectivity over non-CDK kinases, improved cellular activity, and lower plasma clearance. During the fragment to lead process, structural data and LE were

used to ensure optimization was carried out efficiently. It quickly became apparent for indazole based compounds (e.g., **14**) that molecular weight was being added for only small gains in potency. In contrast, introduction of the acetamide moiety to the pyrazole system (**18**) and stabilizing the twisted benzamide conformation (**23**) were very efficient methods of increasing enzyme activity. During later stage lead optimization, LE became a less important criterion as multiple parameters were being changed simultaneously. **28** is a good example of a compound showing a small decrease in enzyme activity, however, this is offset by a change in physicochemical properties leading to an improvement in cellular activity.

Compound **33** is a potent, ligand efficient inhibitor of CDK2 (IC₅₀ = 0.047 μM; LE = 0.42), with good activity against a range of human tumor cell lines. It has a good profile against the major cytochrome P450 isoforms (<30% inhibition at 10 μM for 1A2, 2D6, 3A4, 2C9, 2C19), has good aqueous thermodynamic solubility either as the acetate or hydrochloride salt (>25 mg/ml in water or 0.9% saline), and its synthetic tractability makes it readily amenable to large scale synthesis. On the basis of these and further data (to be published in a later paper), compound **33** was selected as a preclinical development candidate and subsequently entered clinical development.

Experimental Section

Chemistry. Reagents and solvents were obtained from commercial suppliers and used without further purification. Compounds **5–8** were obtained from commercial suppliers. Thin layer chro-

Scheme 4. Key Compounds in the Optimization of Fragment **6** to the Clinical Candidate **33**^a^a IC₅₀ data are for CDK2.

matography (TLC) analytical separations were conducted with E. Merck silica gel F-254 plates of 0.25 mm thickness and were visualized with UV light (254 nm) and/or stained with iodine, potassium permanganate, or phosphomolybdic acid solutions followed by heating. Standard silica gel chromatography was employed as a method of purification using the indicated solvent mixtures. Compound purification was also carried out using a Biotage SP4 system using prepacked disposable SiO₂ cartridges (4, 8, 19, 38, 40, and 90 g sizes) with stepped or gradient elution at 5–40 mL/min of the indicated solvent mixture. Proton nuclear magnetic resonance (¹H NMR) spectra were recorded in the deuterated solvents specified on a Bruker Avance 400 spectrometer operating at 400 MHz. Chemical shifts are reported in parts per million (δ) from the tetramethylsilane internal standard. Data are reported as follows: chemical shift, multiplicity (br = broad, s = singlet, d = doublet, t = triplet, m = multiplet), coupling constants (Hz), integration. Compound purity and mass spectra were determined by a Waters Fractionlynx/Micromass ZQ LC/MS platform using the positive electrospray ionization technique (+ES), or an Agilent 1200SL-6140 LC/MS system using positive–negative switching, both using a mobile phase of acetonitrile/water with 0.1% formic acid (see Supporting Information for experimental details).

4-(6-Chloropyrazin-2-ylamino)benzenesulphonamide (10). A suspension of 2,6-dichloropyrazine (100 mg, 0.67 mmol) and 4-sulfamoyl aniline (115 mg, 0.67 mmol) in NMP in a sealed tube was heated to 250 °C under microwave irradiation for 8 min. The mixture was diluted with water and extracted with EtOAc. The

organic layer was filtered and evaporated under reduced pressure. The residue was purified by preparative HPLC (method C) to give **10** (11 mg, 6%). ¹H NMR (400 MHz, DMSO-*d*₆): δ 10.23 (s, 1H), 8.26 (s, 1H), 8.11 (s, 1H), 7.79 (s, 4H), 7.23 (s, 2H). LC/MS: *R*_t = 1.08 min, [M + H]⁺ 285 (method A).

5-Chloro-7-isopropylaminopyrazolo[1,5-*a*]pyrimidine-3-carbonitrile (11). Isopropylamine (0.12 mL, 2.83 mmol) and potassium carbonate (652 mg, 4.72 mmol) were added to a solution of 5,7-dichloropyrazolo[1,5-*a*]pyrimidine-3-carbonitrile (500 mg, 2.36 mmol) in acetonitrile (10 mL). The resulting mixture was stirred at room temperature overnight, filtered, and concentrated in vacuo to give **11** (10 mg, 2%). ¹H NMR (400 MHz, Me-*d*₃-OD): δ 8.39 (s, 1H), 6.50 (s, 1H), 4.09–3.98 (m, 1H), 1.39 (d, *J* = 6.4 Hz, 6H). LC/MS: *R*_t = 2.81 min, [M + H]⁺ 236 (method A).

5-(4-*trans*-Amino-cyclohexylamino)-7-isopropylamino-pyrazolo[1,5-*a*]pyrimidine-3-carbonitrile formate (12). A solution of 5-chloro-7-isopropylamino-pyrazolo[1,5-*a*]pyrimidine-3-carbonitrile (180 mg, 0.61 mmol), *trans*-1,4-cyclohexanediamine (84 mg 0.73 mmol) and *N,N*-diisopropylethylamine (160 μL) in DMF (3.1 mL) was subjected to microwave heating at 140 °C for 1 h. The reaction mixture was allowed to cool and then purified by RP-HPLC (method C) to afford **12** as a colorless solid (35 mg, 18%). ¹H NMR (400 MHz, DMSO-*d*₆): δ 8.42 (s, 1H), 8.23 (s, 1H), 7.27–7.10 (m, 2H), 5.41 (s, 1H), 3.80 (s, 1H), 3.55 (s, 2H), 2.89 (t, *J* = 12.3 Hz, 1H), 1.96 (t, 4H), 1.46–1.32 (m, 2H), 1.32–1.22 (m, 8H). LC/MS: *R*_t = 1.03 min (RR), [M + H]⁺ 314 (method B).

1*H*-Indazole-3-carboxylic Acid (4-Sulfamoylphenyl)amide (14).

To 1*H*-indazole-3-carboxylic acid (100 mg, 0.6 mmol) in DMF (5 mL) was added EDC (142 mg, 0.72 mmol), HOBt (100 mg, 0.72 mmol), and sulfanilamide (127 mg, 0.72 mmol). The reaction was heated at 100 °C for 48 h then cooled and evaporated. The residue was partitioned between DCM and saturated NaHCO₃ solution, then the resultant solid was collected by filtration, washed with water and DCM, and then dried. The crude material was purified by RP-HPLC (method C), and product containing fractions were combined and evaporated to give **14** as a white solid (12 mg, 6%). ¹H NMR (400 MHz, DMSO-*d*₆): δ 13.87 (s, 1H), 10.68 (s, 1H), 8.24 (d, *J* = 8.1 Hz, 1H), 8.09 (d, *J* = 8.3 Hz, 2H), 7.80 (d, *J* = 8.3 Hz, 2H), 7.69 (d, *J* = 8.4 Hz, 1H), 7.48 (t, *J* = 7.6 Hz, 1H), 7.32 (t, *J* = 7.7 Hz, 1H), 7.26 (s, 2H). LC/MS: *R*_t = 2.72 [M + H]⁺ 317 (method A).

1*H*-Pyrazole-3-carboxylic Acid Phenylamide (15). 1*H*-Pyrazole-3-carboxylic acid (100 mg, 0.9 mmol), EDC (211 mg, 1.1 mmol), HOBt (147 mg, 1.1 mmol), and aniline (0.089 mL, 0.98 mmol) were dissolved in DMF (5 mL) and the resulting solution was stirred for 2 days. The mixture was concentrated under reduced pressure and partitioned between water and EtOAc. The organic fraction was dried (MgSO₄), filtered, and evaporated in vacuo and the residue purified by column chromatography to give **15** (97 mg, 58%) as a white solid. ¹H NMR (400 MHz, DMSO-*d*₆): δ 13.44 (s, 1H), 10.01 (s, 1H), 7.93–7.84 (s, 1H), 7.81 (d, *J* = 8.0 Hz, 2H), 7.33 (dd, 8.0, 7.7 Hz, 2H), 7.08 (t, *J* = 7.7 Hz, 1H), 6.82 (s, 1H). LC/MS: *R*_t = 0.98 (RR) [M – H][–] 186 (method B).

4-Nitro-1*H*-pyrazole-3-carboxylic Acid (4-Fluoro-phenyl)-amide (35). 4-Nitro-1*H*-pyrazole-3-carboxylic acid **34** (10 g; 63.66 mmol) was added to a stirred solution of 4-fluoroaniline (6.7 mL; 70 mmol), EDC (14.6 g; 76.4 mmol), and HOBt (10.3 g; 76.4 mmol) in DMF (25 mL) and then stirred at room temperature for 16 h. The solvent was removed by evaporation under reduced pressure and the residue triturated with EtOAc/saturated brine solution. The resultant yellow solid was collected by filtration, washed with 2 M hydrochloric acid, and then dried under vacuum to give **35** (15.5 g, 97%). ¹H NMR (400 MHz, DMSO-*d*₆): δ 14.25 (s, 1H), 10.73 (s, 1H), 8.96 (s, 1H), 7.72 (dd, *J* = 8.4, 4.9 Hz, 2H), 7.22 (t, *J* = 8.5 Hz, 2H). LC/MS: *R*_t = 2.92 min, [M + H]⁺ 250 (method A).

4-Amino-1*H*-pyrazole-3-carboxylic Acid (4-Fluoro-phenyl)-amide (17). Compound **35** (15 g, 60 mmol) was dissolved in 200 mL of EtOH, treated with 1.5 g of 10% palladium on carbon under a nitrogen atmosphere, then hydrogenated at room temperature and pressure for 16 h. The catalyst was removed by filtration through celite and the filtrate evaporated. The crude product was dissolved in acetone/water (200 mL, 1:1), and after slow evaporation of the acetone, **17** was collected by filtration as a brown crystalline solid (8.1 g, 62%). ¹H NMR (400 MHz, DMSO-*d*₆): δ 12.77 (s, 1H), 9.87 (s, 1H), 7.88–7.76 (m, 2H), 7.25–7.07 (m, 3H), 4.69 (s, 2H). LC/MS: *R*_t = 1.58 min, [M + H]⁺ 221 (method A).

4-Acetylamino-1*H*-pyrazole-3-carboxylic Acid (4-Fluoro-phenyl)-amide (18). Compound **17** (500 mg; 2.27 mmol) was dissolved in pyridine (5 mL), treated with acetic anhydride (240 μL, 2.5 mmol), and then stirred at room temperature for 16 h. The solvent was removed by evaporation, and then dichloromethane (20 mL) and 2 M hydrochloric acid (20 mL) were added. The undissolved solid was collected by filtration, washed with dichloromethane and water, and then dried under vacuum. The product **18** was isolated as an off-white solid (275 mg, 46%). ¹H NMR (400 MHz, DMSO-*d*₆): δ 13.33 (br s, 1H), 10.29 (s, 1H), 9.54 (s, 1H), 8.24 (s, 1H), 7.90–7.77 (m, 2H), 7.18 (t, *J* = 8.7 Hz, 2H), 2.12 (s, 3H). LC/MS: *R*_t = 2.96 min, [M + H]⁺ 263 (method A).

4-(2-Hydroxyacetylamino)-1*H*-pyrazole-3-carboxylic Acid (4-fluorophenyl)amide (19). Hydroxyacetic acid (19 mg, 0.25 mmol) was added to a solution of **17** (50 mg, 0.23 mmol), EDC (53 mg, 0.27 mmol), and HOBt (37 mg, 0.27 mmol) in DMF (5 mL). The reaction mixture was stirred at room temperature for 24 h. The solvent was removed under reduced pressure. The residue was purified by preparative LC/MS (method C) and, after evaporation of product-containing fractions, yielded **19** as a white solid (26 mg, 41%). ¹H NMR (400 MHz, DMSO-*d*₆): δ 13.45 (s, 1H), 10.42 (s,

1H), 10.37 (s, 1H), 8.38–8.26 (m, 1H), 7.92–7.79 (m, 2H), 7.25–7.12 (m, 2H), 6.09 (t, *J* = 5.6 Hz, 1H), 4.01 (d, *J* = 5.6 Hz, 2H). LC/MS: *R*_t = 2.65 min, [M + H]⁺ 278 (method A).

The following compounds were synthesized using the same method as used for **19**:

4-Benzoylamino-1*H*-pyrazole-3-carboxylic Acid (4-Fluoro-phenyl)-amide (22). Benzoic acid gave **22** as a pink solid (26 mg, 35%). ¹H NMR (400 MHz, DMSO-*d*₆): δ 13.55 (br s, 1H), 10.56 (s, 1H), 10.50 (s, 1H), 8.42 (s, 1H), 7.96–7.81 (m, 4H), 7.70–7.55 (m, 3H), 7.27–7.14 (m, 2H). LC/MS: *R*_t = 3.96 min, [M + H]⁺ 324 (method A).

4-(2,6-Difluoro-benzoylamino)-1*H*-pyrazole-3-carboxylic Acid (4-Fluoro-phenyl)-amide (23). 2,6-Difluorobenzoic acid in DMSO gave **23** as a cream-colored solid (25 mg, 30%). ¹H NMR (400 MHz, DMSO-*d*₆): δ 13.57 (s, 1H), 10.42 (s, 1H), 10.31 (s, 1H), 8.43 (s, 1H), 7.88–7.77 (m, 2H), 7.69–7.58 (m, 1H), 7.27 (dd, *J* = 8.6, 8.5 Hz, 2H), 7.17 (dd, *J* = 8.7, 8.6 Hz, 2H). LC/MS: *R*_t = 3.76 min, [M + H]⁺ 361 (method A).

4-Amino-1*H*-pyrazole-3-carboxylic Acid Ethyl Ester (36). Step 1. Thionyl chloride (2.9 mL, 39.8 mmol) was slowly added to a mixture of **34** (5.68 g, 36.2 mmol) in EtOH (100 mL) at room temperature then stirred for 48 h. The mixture was evaporated in vacuo and re-evaporated with toluene to afford 4-nitro-1*H*-pyrazole-3-carboxylic acid ethyl ester as a white solid (6.42 g, 96%). ¹H NMR (400 MHz, DMSO-*d*₆): δ 14.4 (s, 1H), 9.0 (s, 1H), 4.4 (q, 2H), 1.3 (t, 3H).

Step 2. A mixture of 4-nitro-1*H*-pyrazole-3-carboxylic acid ethyl ester (6.40 g, 34.6 mmol) and 10% Pd/C (650 mg) in EtOH (150 mL) was stirred under an atmosphere of hydrogen for 20 h. The mixture was filtered through a plug of celite, evaporated under vacuum then re-evaporated with toluene to afford **36** as a pink solid (5.28 g, 98%). ¹H NMR (400 MHz, DMSO-*d*₆): δ 12.7 (s, 1H), 7.1 (s, 1H), 4.8 (s, 2H), 4.3 (q, 2H), 1.3 (t, 3H) (method A).

4-(2,6-Difluoro-benzoylamino)-1*H*-pyrazole-3-carboxylic Acid (37). A mixture of 2,6-difluorobenzoic acid (6.32 g, 40.0 mmol), **36** (5.96 g, 38.4 mmol), EDC (8.83 g, 46.1 mmol), and HOBt (6.23 g, 46.1 mmol) in DMF (100 mL) was stirred at ambient temperature for 6 h. The mixture was reduced in vacuo, water added, and the solid formed collected by filtration and air-dried to give 4-(2,6-difluoro-benzoylamino)-1*H*-pyrazole-3-carboxylic acid ethyl ester as the major component of a mixture (15.3 g). LC/MS: *R*_t = 3.11 min, [M + H]⁺ 295. Crude 4-(2,6-difluoro-benzoylamino)-1*H*-pyrazole-3-carboxylic acid ethyl ester (10.2 g) in 2 M aqueous NaOH/MeOH (1:1, 250 mL) was stirred at ambient temperature for 14 h. Volatile materials were removed in vacuo, water (300 mL) added and the mixture adjusted to pH 5 using 1 M aqueous HCl. The resultant precipitate was collected by filtration and dried through azeotrope with toluene to afford **37** as a pink solid (5.70 g, 83% from **36**). ¹H NMR (400 MHz, DMSO-*d*₆): δ 13.60–13.30 (br s, 1H), 10.06 (s, 1H), 8.25 (s, 1H), 7.68–7.54 (m, 1H), 7.25 (t, *J* = 8.4 Hz, 2H). LC/MS: *R*_t = 2.33 min (94% purity), [M + H]⁺ 267 (method A).

4-(2,6-Difluoro-benzoylamino)-1*H*-pyrazole-3-carboxylic Acid (trans-4-Amino-cyclohexyl)-amide (27). A mixture of **37** (100 mg, 0.37 mmol), (*trans*-4-amino-cyclohexyl)-carbamic acid *tert*-butyl ester (98 mg, 0.46 mmol), EDC (86 mg, 0.45 mmol), and HOBt (60 mg, 0.45 mmol) in DMSO (5 mL) was stirred at ambient temperature for 16 h. The mixture was reduced in vacuo, then the residue taken up in CH₂Cl₂ and washed successively with saturated aqueous sodium bicarbonate, water, and brine. The organic portion was dried (MgSO₄), filtered, and the solvent reduced in vacuo. Trituration of the resulting solid with CH₂Cl₂ gave **27**, protected with an *N*-*tert*-butoxycarbonyl (*t*-Boc) group. This was removed by treatment with saturated EtOAc/HCl at room temperature for 1 h. The solid that precipitated out of the reaction mixture was filtered off, washed with ether, and then dried to give **27** (14 mg, 10%). ¹H NMR (400 MHz, Me-*d*₃-OD): δ 8.45 (s, 1H), 8.36 (s, 1H), 7.63–7.57 (m, 1H), 7.16 (t, *J* = 8.6 Hz, 2H), 3.91–3.84 (m, 1H), 3.18–3.11 (m, 1H), 2.16–2.05 (m, 4H), 2.03 (s, 1H), 1.61–1.50 (m, 4H). LC/MS: *R*_t = 1.75 min, [M + H]⁺ 364 (method A).

The following compounds were synthesized in an analogous manner to **27**:

4-(2,6-Difluoro-benzoylamino)-1H-pyrazole-3-carboxylic Acid Piperidin-4-ylamide (28). 4-Amino-piperidine-1-carboxylic acid *tert*-butyl ester gave **28** (62 mg, 48%). ¹H NMR (400 MHz, DMSO-*d*₆): δ 13.49 (s, 1H), 10.38 (s, 1H), 9.08 (br d, 1H), 8.69 (br s, 2H), 8.32 (s, 1H), 7.69–7.58 (m, 1H), 7.27 (t, *J* = 8.6 Hz, 2H), 4.11–3.96 (m, 1H), 3.28 (d, 2H), 3.01–2.88 (m, 2H), 2.00–1.75 (m, 4H). LC/MS: *R*_t = 1.57 min, [M + H]⁺ 350 (method A).

4-(2,6-Difluoro-benzoylamino)-1H-pyrazole-3-(S)-carboxylic Acid Piperidin-3-(S)-ylamide Hydrochloride (29). Using HOAt instead of HOBt, 3-(S)-amino-piperidine-1-carboxylic acid *tert*-butyl ester gave **29** (55 mg, 43%). ¹H NMR (400 MHz, Me-*d*₃-OD): δ 8.37 (s, 1H), 8.35 (s, 1H), 7.65–7.56 (m, 1H), 7.17 (t, *J* = 8.6 Hz, 2H), 4.32–4.22 (m, 1H), 3.49 (dd, *J* = 12.2, 4.1, 1H), 3.36 (s, 1H), 3.08–2.94 (m, 2H), 2.15–2.02 (m, 2H), 1.92–1.73 (m, 2H). LC/MS: *R*_t = 1.76 min, [M + H]⁺ 350 (method A).

4-[(4-Amino-1H-pyrazole-3-carbonyl)-amino]-piperidine-1-carboxylic Acid *tert*-Butyl Ester (38).

Step 1. A solution of **34** (7.3 g, 45.8 mmol), 4-amino-piperidine-1-carboxylic acid *tert*-butyl ester (10.2 mg, 51 mmol), EDC (10.7 g, 55.8 mmol), and HOAt (7.5 g, 55.8 mmol) in DMF (100 mL), was stirred at room temperature for 16 h. The solvent was then removed by evaporation under reduced pressure and the residue triturated with water (250 mL). The resultant cream solid was collected by filtration, washed with water, and then dried under vacuum to give 4-[(4-nitro-1H-pyrazole-3-carbonyl)-amino]-piperidine-1-carboxylic acid *tert*-butyl ester (13.05 g, 84%). ¹H NMR (400 MHz, DMSO-*d*₆): δ 12.53 (s, 1H), 7.67 (d, *J* = 8.4 Hz, 1H), 7.10 (s, 1H), 4.60–4.52 (m, 1H), 3.99–3.83 (b m, 4H), 2.88–2.75 (m, 2H), 1.74–1.68 (m, 2H), 1.52–1.37 (m, 11H). LC/MS: *R*_t = 2.50 min, [M + H]⁺ 340 (method A).

Step 2. 4-[(4-Nitro-1H-pyrazole-3-carbonyl)-amino]-piperidine-1-carboxylic acid *tert*-butyl ester (13.05 g, 38.4 mmol) was dissolved in EtOH (300 mL) and DMF (75 mL), treated with 10% palladium on carbon (500 mg) and then hydrogenated at room temperature and pressure for 16 h. The catalyst was removed by filtration through celite, the filtrate evaporated and re-evaporated with toluene. The crude material was purified by flash column chromatography eluting with EtOAc then 2% MeOH/EtOAc then 5% MeOH/EtOAc. Product containing fractions were combined and evaporated to give **38** (8.78 g, 74%) as a brown foam. ¹H NMR (400 MHz, DMSO-*d*₆): δ 12.53 (s, 1H), 7.67 (d, *J* = 8.4 Hz, 1H), 7.10 (s, 1H), 4.60–4.50 (m, 1H), 3.98–3.81 (m, 4H), 2.87–2.81 (m, 2H), 1.76–1.66 (m, 2H), 1.54–1.35 (m, 11H). LC/MS: *R*_t = 1.91 min, [M + H]⁺ 310 (method A).

Compound 33 was Made Using the Following General Method.

To a stirred solution of **38** (0.23 mmol), EDC (52 mg; 0.27 mmol), and HOBt (37 mg; 0.27 mmol) in DMF (5 mL) was added the corresponding carboxylic acid (0.25 mmol), and the mixture was then left at room temperature for 16 h. The reaction mixture was evaporated and the residue purified by flash column chromatography or preparative LC/MS. The compound was treated with saturated EtOAc/HCl and stirred at room temperature for 1 h. The precipitated solid was filtered off, washed with ether, and then dried to give the required product.

4-(2,6-Dichloro-benzoylamino)-1H-pyrazole-3-carboxylic Acid Piperidin-4-ylamide Hydrochloride (33). 2,6-Dichlorobenzoic acid gave **33** (64 mg, 73%). ¹H NMR (400 MHz, Me-*d*₃-OD): δ 8.37 (s, 1H), 7.57–7.43 (m, 3H), 4.22–4.08 (m, 1H), 3.53–3.40 (m, 2H), 3.22–3.07 (m, 2H), 2.25–2.12 (m, 2H), 1.99–1.80 (m, 2H). LC/MS: *R*_t = 1.87 min, [M + H]⁺ 383 (method A).

Crystallography. Crystals of CDK2 were produced using published protocols.^{47,48} Soaking of ligands into CDK2 crystals, data collection, ligand fitting, structure refinement, and structure rebuilding were performed using methods described by Hartshorn et al.¹

Biological Assays and DMPK studies. Detailed experimental details can be found in the Supporting Information.

Acknowledgment. We thank Emma Vickerstaffe and Charlotte Griffiths-Jones for writing the experimental details, Miles Congreve, Martyn Frederickson, Emma Vickerstaffe, Michelle Jones, and Chris Murray for proof reading, and David Rees, Nicola Wallis, and Neil Thompson for useful discussions. We are also grateful to Molecular Imaging Research Inc (Ann Arbor, MI), particularly W. R. Leopold, III, and Erin Trachet, for conducting the xenograft studies using SCID mice.

Supporting Information Available: In vitro kinase selectivity data; detailed descriptions of HPLC methods; HPLC purity analysis of final compounds; NMR spectra and HPLC traces for compounds **10**, **12**, **14**, **15**, **18**, **22**, **23**, **28**, **33**; further synthetic chemistry experimental; experimental details for biological assays and DMPK studies. This material is available free of charge via the Internet at <http://pubs.acs.org>.

References

- Hartshorn, M. J.; Murray, C. W.; Cleasby, A.; Frederickson, M.; Tickle, I. J.; Jhoti, H. Fragment-Based Lead Discovery Using X-ray Crystallography. *J. Med. Chem.* **2005**, *48*, 403–413.
- Gill, A. L.; Frederickson, M.; Cleasby, A.; Woodhead, S. J.; Carr, M. G.; Woodhead, A. J.; Walker, M. T.; Congreve, M. S.; Devine, L. A.; Tisi, D.; O'Reilly, M.; Seavers, L. C. A.; Davis, D. J.; Curry, J.; Anthony, R.; Padova, A.; Murray, C. W.; Carr, R. A. E.; Jhoti, H. Identification of Novel p38α MAP Kinase Inhibitors Using Fragment-Based Lead Generation. *J. Med. Chem.* **2005**, *48*, 414–426.
- Jahnke, W.; Erlanson, D. A. *Fragment-Based Approaches in Drug Discovery*; Wiley: Weinheim, Germany, 2007.
- Congreve, M.; Chessari, G.; Tisi, D.; Woodhead, A. J. Recent developments in fragment-based drug discovery. *J. Med. Chem.* **2008**, *51*, 3661–3680.
- Ciulli, A.; Abell, C. Fragment-based approaches to enzyme inhibition. *Curr. Opin. Biotechnol.* **2007**, *18*, 489–496.
- Congreve, M.; Murray, C. W.; Carr, R.; Rees, D. C. Fragment-based lead discovery. In *Annual Reports in Medicinal Chemistry*; Elsevier Inc.: New York, 2007; pp 431–448.
- Hajduk, P. J.; Greer, J. A. decade of fragment-based drug design: strategic advances and lessons learned. *Nat. Rev. Drug Discovery* **2007**, *6*, 211–219.
- Lesuisse, D.; Lange, G.; Deprez, P.; Bernard, D.; Schoot, B.; Delettre, G.; Marquette, J. P.; Broto, P.; Jean-Baptiste, V.; Bichet, P.; Sarubbi, E.; Mandine, E. SAR and X-ray. A new approach combining fragment-based screening and rational drug design: application to the discovery of nanomolar inhibitors of Src SH2. *J. Med. Chem.* **2002**, *45*, 2379–2387.
- Lepre, C. A.; Moore, J. M.; Peng, J. W. Theory and applications of NMR-based screening in pharmaceutical research. *Chem. Rev.* **2004**, *104*, 3641–3676.
- Neumann, T.; Junker, H. D.; Schmidt, K.; Sekul, R. SPR-based fragment screening: advantages and applications. *Curr. Top. Med. Chem.* **2007**, *7*, 1630–1642.
- Hann, M. M.; Leach, A. R.; Harper, G. Molecular complexity and its impact on the probability of finding leads for drug discovery. *J. Chem. Inf. Comput. Sci.* **2001**, *41*, 856–864.
- Hopkins, A. L.; Groom, C. R.; Alex, A. Ligand efficiency: a useful metric for lead selection. *Drug Discovery Today* **2004**, *9*, 430–431.
- Sherr, C. J. Cancer Cell Cycles. *Science* **1996**, *274*, 672–677.
- Grana, X.; Reddy, E. P. Cell cycle control in mammalian cells: role of cyclins, cyclin-dependent kinases (CDKs), growth suppressor genes and cyclin-dependent kinase inhibitors (CKIs). *Oncogene* **1995**, *11*, 211–9.
- Morgan, D. Principles of CDK regulation. *Nature* **1995**, *374*, 131–134.
- Hall, M.; Peters, G. Genetic alterations of cyclins, cyclin dependent kinases and Cdk inhibitors in human cancer. *Adv. Cancer Res.* **1996**, *68*, 67–108.
- Van den Heuvel, S.; Harlow, E. Distinct roles for cyclin-dependent kinases in cell cycle control. *Science* **1993**, *262*, 2050–2054.
- Malumbres, M.; Barbacid, M. To cycle or not to cycle: a critical decision in cancer. *Nat. Rev. Cancer* **2001**, *1*, 222–231.
- Ortega, S.; Malumbres, M.; Barbacid, M. Cyclin D-dependent kinases, INK4 inhibitors and cancer. *Biochim. Biophys. Acta* **2002**, *602*, 73–87.
- Weinberg, R. A. The retinoblastoma protein and cell cycle control. *Cell* **1995**, *81*, 323–330.

- (21) Zhao, J.; Dynlacht, B.; Imai, T.; Hori, T.; Harlow, E. Expression of NPAT, a novel substrate of cyclin E-CDK2, promotes S-Phase entry. *Genes Dev.* **1998**, *12*, 456–461.
- (22) Zhao, J.; Kennedy, B. K.; Lawrence, B. D.; Barbie, D. A.; Matera, A. G.; Fletcher, J. A.; Harlow, E. NPAT links cyclin E-CDK2 to the regulation of replication-dependent histone gene transcription. *Genes Dev.* **2000**, *14*, 2283–2297.
- (23) Santoni-Rugiu, E.; Falck, J.; Mailand, N.; Bartek, J.; Lukas, J. Involvement of Myc activity in a G1/S-promoting mechanism parallel to the pRb/E2F pathway. *Mol. Cell. Biol.* **2000**, *20*, 3497–3509.
- (24) Obaya, A. J.; Kottenko, I.; Cole, M. D.; Sedivy, J. M. The proto-oncogene *cmyc* acts through the cyclin-dependent kinase (CDK) inhibitor p27^{KIP1} to facilitate the activation of CDK4/6 and early G1 phase progression. *J. Biol. Chem.* **2002**, *277*, 31263–31269.
- (25) Dynlacht, B. Regulation of transcription during the cell cycle. *Transcription Factors* **2001**, *85*, 112.
- (26) De Falco, G.; Giordano, A. CDK9: from basal transcription to cancer and AIDS. *Cancer Biol. Therap.* **2002**, *1*, 342–347.
- (27) Cruz, J. C.; Tsai, L. A. Jekyll and Hyde kinase: roles for CDK5 in brain development and disease. *Curr. Opin. Neurobiol.* **2004**, *14*, 390–394.
- (28) Berthet, C.; Aleem, E.; Coppola, V.; Tessarollo, L.; Kaldis, P. CDK2 knockout mice are viable. *Curr. Biol.* **2003**, *13*, 1775–1785.
- (29) Tetsu, O.; McCormick, F. Proliferation of cancer cells despite CDK2 inhibition. *Cancer Cell* **2003**, *3*, 233–245.
- (30) Ortega, S.; Prieto, I.; Odajima, J.; Martin, A.; Dubus, P.; Sotillo, R.; Barbero, J. L.; Malumbres, M.; Barbacid, M. Cyclin-dependent kinase 2 is essential for meiosis but not for mitotic cell division in mice. *Nat. Genet.* **2003**, *35*, 25–31.
- (31) Geng, Y.; Yu, Q.; Sicinska, E.; Das, M.; Schneider, J. E.; Bhattacharya, S.; Rideout, W. M., III; Bronson, R. T.; Gardner, H.; Sicinski, P. Cyclin E ablation in the mouse. *Cell* **2003**, *114*, 431–443.
- (32) Malumbres, M.; Sotillo, R.; Santamaria, D.; Galan, J.; Cerezo, A.; Ortega, S.; Dubus, P.; Barbacid, M. Mammalian cells cycle without the D-type cyclin-dependent kinases CDK4 and CDK6. *Cell* **2004**, *118*, 493–504.
- (33) Sharma, S. P.; Sharma, R.; Tyagi, R. Inhibitors of cyclin dependent kinases: useful targets for cancer treatment. *Curr. Cancer Drug Targets* **2008**, *8*, 53–75.
- (34) Pevarello, P.; Villa, M. Cyclin-dependent kinase inhibitors: a survey of the recent patent literature. *Expert Opin. Ther. Pat.* **2005**, *15*, 675–703.
- (35) Christian, B. A.; Grever, M. R.; Byrd, J. C.; Lin, T. S. Flavopiridol in the treatment of chronic lymphocytic leukemia. *Curr. Opin. Oncol.* **2007**, *19*, 573–578.
- (36) Fuse, E.; Kuwabara, T.; Sparreboom, A.; Sausville, E. A.; Figg, W. D. Review of UCN-01 development: A lesson in the importance of clinical pharmacology. *J. Clin. Pharm.* **2005**, *45*, 394–403.
- (37) Alvocidib: orphan drug status. U.S. Food and Drug Administration, Committee for Orphan Medicinal Products 84th Plenary Meeting, 2007.
- (38) Meijer, L.; Bettayeb, K.; Galons, H. (R)-roscovitine (CYC202, seliciclib). In *Inhibitors of Cyclin-Dependent Kinases as Anti-Tumor Agents*; CRC: Boca Raton, FL, 2007; pp 187–225.
- (39) Misra, R. N.; Xiao, H.; Kim, K. S.; Lu, S.; Han, W.; Barbosa, S. A.; Hunt, J. T.; Rawlins, D. B.; Shan, W.; Ahmed, S. Z.; Qian, L.; Chen, B.; Zhao, R.; Bednarz, M. S.; Kellar, K. A.; Mulheron, J. G.; Batorsky, R.; Roongta, U.; Kamath, A.; Marathe, P.; Ranadive, S. A.; Sack, J. S.; Tokarski, J. S.; Pavletich, N. P.; Lee, F. Y. F.; Webster, K. R.; Kimball, S. D. *N*-(cycloalkylamino)acyl-2-aminothiazole inhibitors of cyclin-dependent kinase 2. *N*-[5-[[[5-(1,1-dimethylethyl)-2-oxazolyl]methyl]thio]-2-thiazolyl]-4-piperidinecarboxamide (BMS-387032), a highly efficacious and selective antitumor agent. *J. Med. Chem.* **2004**, *47*, 1719–1728.
- (40) Toogood, P. L.; Harvey, P. J.; Repine, J. T.; Sheehan, D. J.; VanderWel, S. N.; Zhou, H.; Keller, P. R.; McNamara, D. J.; Sherry, D.; Zhu, T.; Brodfuehrer, J.; Choi, C.; Barvian, M. R.; Fry, D. W. Discovery of a Potent and Selective Inhibitor of Cyclin-Dependent Kinase 4/6. *J. Med. Chem.* **2005**, *48*, 2388–2406.
- (41) Hennequin, L. F.; Allen, J.; Breed, J.; Curwen, J.; Fennell, M.; Green, T. P.; Lambert-van der Bempt, C.; Morgentin, R.; Norman, R. A.; Olivier, A.; Otterbein, L.; Ple, P. A.; Warin, N.; Costello, G. *N*-(5-chloro-1,3-benzodioxol-4-yl)-7-[2-(4-methylpiperazin-1-yl)ethoxy]-5-(tetrahydro-2*H*-pyran-4-yloxy)quinazolin-4-amine, a novel, highly selective, orally available, dual-specific c-Src/Abl kinase inhibitor. *J. Med. Chem.* **2006**, *49*, 6465–6488.
- (42) Bramson, H. N.; Corona, J.; Davis, S. T.; Dickerson, S. H.; Edelman, M.; Frye, S. V.; Gampe, R. T., Jr.; Harris, P. A.; Hassell, A.; Holmes, W. D.; Hunter, R. N.; Lackey, K. E.; Lovejoy, B.; Luzzio, M. J.; Montana, V.; Rocque, W. J.; Rusnak, D.; Shewchuk, L.; Veal, J. M.; Walker, D. H.; Kuyper, L. F. Oxindole-Based Inhibitors of Cyclin-Dependent Kinase 2 (CDK2): Design, Synthesis, Enzymatic Activities, and X-ray Crystallographic Analysis. *J. Med. Chem.* **2001**, *44*, 4339–4358.
- (43) Byth, K. F.; Culshaw, J. D.; Green, S.; Oakes, S. E.; Thomas, A. P. Imidazo[1,2-*a*]pyridines. Part 2: SAR and optimisation of a potent and selective class of cyclin-dependent kinase inhibitors. *Bioorg. Med. Chem. Lett.* **2004**, *14*, 2245–2248.
- (44) Liao, J. Molecular recognition of protein kinase binding pockets for design of potent and selective kinase inhibitors. *J. Med. Chem.* **2007**, *50*, 409–424.
- (45) Barvian, M.; Boschelli, D.; Cossrow, J.; Dobrusin, E.; Fattaey, A.; Fritsch, A.; Fry, D.; Harvey, P.; Keller, P.; Garrett, M.; La, F.; Leopold, W.; McNamara, D.; Quin, M.; Trumpp-Kallmeyer, S.; Toogood, P.; Wu, Z.; Zhang, E. Pyrido[2,3-*d*]pyrimidin-7-one Inhibitors of Cyclin-Dependent Kinases. *J. Med. Chem.* **2000**, *43*, 4606–4616.
- (46) Honma, T.; Hayashi, K.; Aoyama, T.; Hashimoto, N.; Machida, T.; Fukasawa, K.; Iwama, T.; Ikeura, C.; Ikuta, M.; Suzuki-Takahashi, I.; Iwasawa, Y.; Hayama, T.; Nishimura, S.; Morishima, H. Structure-Based Generation of a New Class of Potent Cdk4 Inhibitors New de Novo Design Strategy and Library Design. *J. Med. Chem.* **2001**, *44*, 4615–4627.
- (47) Meijer, L.; Borgne, A.; Mulner, O.; Chong, J. P. J.; Blow, J. J.; Inagaki, N.; Inagaki, M.; Delcros, J. G.; Moulinoux, J. P. Biochemical and cellular effects of roscovitine, a potent and selective inhibitor of the cyclin-dependent kinases *cdc2*, *cdk2*, and *cdk5*. *Eur. J. Biochem.* **1997**, *243*, 527–536.
- (48) Schulze-Gahmen, U.; De Bondt, H. L.; Kim, S. H. High-resolution crystal structures of human cyclin-dependent kinase 2 with and without ATP: bound waters and natural ligand as guides for inhibitor design. *J. Med. Chem.* **1996**, *39*, 4540–4546.
- (49) Brown, N. R.; Noble, M. E. M.; Endicott, J. A.; Johnson, L. N. The structural basis for specificity of substrate and recruitment peptides for cyclin-dependent kinases. *Nat. Cell Biol.* **1999**, *1*, 438–443.
- (50) Lowe, E. D.; Tews, I.; Cheng, K. Y.; Brown, N. R.; Gul, S.; Noble, M. E. M.; Gamblin, S. J.; Johnson, L. N. Specificity Determinants of Recruitment Peptides Bound to Phospho-CDK2/Cyclin A. *Biochemistry* **2002**, *41*, 15625–15634.
- (51) Nociari, M. M.; Shalev, A.; Benias, P.; Russo, C. A novel one-step, highly sensitive fluorometric assay to evaluate cell-mediated cytotoxicity. *J. Immunol. Methods* **1998**, *213*, 157–167.
- (52) Tisi, D.; Chessari, G.; Woodhead, A. J.; Jhoti, H. Structural biology and anticancer drug design. In *Cancer Drug Design and Discovery*; Elsevier: New York, 2008; pp 91–106.

JM800382H